Electric-Field Adjustable Time-Dependent Magnetoelectric Response in Martensitic FeRh Alloy

Ignasi Fina,[a] Alberto Quintana,[b] Jessica Padilla-Pantoja,[c] Xavier Martí,[d], Ferran Macià,[a] Florencio Sánchez,[a] Michael Foerster,[e] Lucia Aballe,[e] Josep Fontcuberta,[a] Jordi Sort[b,f]*

[a]Institut de Ciència de Materials de Barcelona (ICMAB-CSIC), Campus UAB, E-08193 Bellaterra, Barcelona, Spain

[b]Departament de Física, Universitat Autònoma de Barcelona, E-08193 Bellaterra, Barcelona, Spain

[c]Catalan Institute of Nanoscience and Nanotechnology (ICN2), CSIC and The Barcelona Institute of Science and Technology, Campus UAB, E-08193 Bellaterra, Barcelona, Spain

[d]Institute of Physics, Academy of Sciences of the Czech Republic, Cukrovarnická 10, 162 53 Praha 6, Czech Republic

[e]ALBA Synchrotron Light Facility, Carrer de la Llum 2-26, Cerdanyola del Vallès, Barcelona 08290, Spain

[f]Institució Catalana de Recerca i Estudis Avançats (ICREA), Pg. Lluís Companys 23, E-08010 Barcelona, Spain

Keywords: multiferroic; magnetoelectric; martensitic alloy; thin film; piezoelectric

Abstract:

Steady or dynamic magnetoelectric response, selectable and adjustable by only varying the amplitude of an applied electric field, is found in a multiferroic FeRh/PMNPT device. In-operando time-dependent structural, ferroelectric and magnetoelectric characterizations provide evidence that, as in magnetic shape-memory martensitic alloys, the observed distinctive magnetoelectric responses are related to the time-dependent relative abundance of antiferromagnetic-ferromagnetic phases in FeRh, unbalanced by voltage-controlled strain. This flexible magnetoelectric response can be exploited not only for energy efficient memory operations but also in other applications where multilevel and/or transient responses are required.

Introduction

During the last decades, a flurry of research in spintronics has focused on finding a system where the net magnetization can be controlled by electric field without the need of electric current, hence largely overcoming power dissipation by Joule heating.[1] Multiferroic oxides and related heterostructures have been pivotal in this race,[2-5] by exploiting the steady magnetoelectric (SME) coupling among distinct ferroic orders. On the other hand, dynamic magnetoelectric (DME) coupling effects, those showing time dependence magnetic response to the electric field, have been observed in a few multiferroic single-phase systems only at low temperatures[6-11]. DME effects in single phase multiferroic systems, can be broadly categorized depending on its origin as arising from: i) coexistence of competing multiferroic domain structures,[6-9] ii) multiferroic domain walls,[10] or iii) electric excitation of magnetic waves.[10-11] Heterostructures with possible

appearance of room-temperature DME coupling have been theoretically suggested but not experimentally realized yet.[12]

Here we explore a radically different approach to obtain a DME above room temperature. Inspired by the physics underneath shape-memory martensitic alloys, we take advantage of the α'-FeRh first order transition, from antiferromagnetic (AFM) to ferromagnetic (FM) states, that occurs at the Néel temperature ($T_N \approx$ 75-105 °C). A coexistence of AFM and FM nanoregions near T_N, together with thermal hysteresis, have been documented in this system.[13-14] The unit cell volume expansion (~1%)[15] of FeRh at the transition point has been exploited to achieve SME by electric modulation of the relative concentration of FM and AFM phases using piezoelectric substrates.[16-17] Importantly, FeRh alloys are known to display remarkably large magnetocaloric and elastocaloric effects,[18] both associated to the martensitic nature of the AFM-FM phase transition. The martensitic character of the FeRh phase transition anticipates a particular DME response to electric/strain stimuli, which has not been explored yet.

In the present work, either SME or DME responses, adjustable by modifying the amplitude of an applied electric field, are found in a FeRh/piezoelectric device. Time-dependent structural and magnetoelectric characterizations as well as direct magnetic domain imaging using X-ray magnetic circular dichroism (XMCD), under *in-operando* conditions have shown that the DME effect arises from the time-dependent evolution of the relative abundance of AFM and FM phases obtained after suitable electric field poling.

Results and Discussion

The central result of our work is shown in **Figure 1**. We measured the time dependence of the magnetoelectric effect of a 50 nm thick FeRh film grown on top of a ferroelectric (0.72)[$PbMg_{1/3}Nb_{2/3}O_3$]-(0.28)[$PbTiO_3$] (PMNPT) (001)-oriented single-crystal substrate. Isothermal measurements were performed at 110 °C (i.e., near the AFM-FM phase transition with coexistence of both phases) and at magnetic remanence ($\mu_0 H = 0$, see detailed explanation on sample preparation in Supporting Information Figure S1). The time-dependent in-plane magnetic moment [$m(t,V)$] was recorded while applying voltage pulse $V(t)$ trains (using Vibrating Sample Magnetometer platform from MicroSense Co) as illustrated in Figure 1a using the electric configuration shown in Figure 1b. First, the PMNPT substrate was poled by a voltage large enough to saturate its polar state, applied for 10 s (from -10 s to 0 s in Figure 1a). Subsequently, longer voltage pulse (0 s - 80 s in Figure 1a) of different magnitudes (V) where applied to the sample. Finally, the bias voltage was zeroed at 80 s. Illustrative $m(t,V)$ data for selected V values are shown in Figure 1c. It can be appreciated that for small V ($V \leq 50$ V) there is no discernible change of $m(t)$, and the initial magnetic moment remains constant ($m_0 \approx 20$ μemu, curves labelled 0-50 V in Figure 1c). Conversely, for intermediate voltages 55 V $\leq V <$ 80 V, remarkable changes in $m(t)$ are detected and, importantly, the time-dependent $m(t,V)$ is found to be different depending on V. Indeed, for 55 V $\leq V \leq$ 60 V, the magnetic moment increases with V, it becomes time-independent and the $m(t,V)$ value set by the V-bias remains constant after the applied voltage is zeroed (at t = 80 s). This implies that a non-volatile magnetic state has been written (see Supporting Information Figure S2). In contrast, when applying a larger V (60 V $< V \leq$ 70 V), although a comparable initial increase of magnetic moment is observed, a striking decay of $m(t,V)$ is well visible (even while keeping V applied) until the initial m_0 is recovered,

with a time constant of about $\tau \approx 10$ s (see Supporting Information Figure S3). Applying much larger voltages (i.e., $V = 100$ V, bottom panel in Figure 1c) results in no observable changes in $m(t,V)$. Therefore, depending on the applied voltage, three regions in the magnetoelectric response are identified (Figure 1d): **I)** $55\ \text{V} \leq V \leq 60\ \text{V}$, the magnetoelectric response is **steady and persistent**, the magnetic moment increases with V and this modification is non-volatile; **II)** $60\ \text{V} < V < 80\ \text{V}$, the magnetoelectric response is **dynamic**, $m(t,V)$ increases with V but it subsequently decays; **III)** $V < 55$ V and $V > 80$ V, applied voltage does not produce visible changes of magnetic moment (**no-magnetoelectric** response**)**. These results are independent of the polarity of the V-bias (see Supporting Information Figure S4).

Complementary magnetoelectric and X-ray diffraction (XRD) experiments of the steady response (region **I**) indicate that the magnetoelectric effect is dominated by strain coupling between FeRh and the PMNPT substrate (see Supporting Information Figure S5), in agreement with earlier reports,[16-17, 19-21] and disregarding the role of possible ion migration[22-24] or other effects not related to strain to be at the origin of the observed magnetoelectric response. To get insight on the strikingly different and novel time-dependent magnetoelectric response observed in region **II,** time-dependent ferroelectric and structural characterizations were performed (**Figure 2**). First, we measured ferroelectric polarization loops (at 110 ^{o}C), using voltage pulses of frequencies of 0.005 and 1 Hz (Figure 2a). The polarization values recorded at both frequencies coincide, revealing that the time-scale for polarization switching is shorter than 1 s. This observation rules out the possibility that the ferroelectric polarization switching process and the associated strain variation could be responsible for the much slower transient response observed in Figure 1c. Note that the coercive voltage ($V_C = 60$ V) is coincident with the voltage at which maximum SME is observed.

Next, we explored the possible role of the kinetics of the AFM-FM phase transition on the time-dependent magnetoelectric response. To analyze the AFM-FM phase transition in *in-operando* conditions, time-dependent θ-2θ XRD scans around the (110) - FeRh reflection were collected (at 110 °C). In Figure 2b we show the corresponding data acquired after applying 65 V at $t_S = 0$ and waiting for $t_S = 5$ s and 75 s prior to start the θ-2θ scan. Lines through data points correspond to Gaussian fits of the data. Careful data inspection indicates a slight shift of the (110) FeRh reflection towards smaller angles with time. This is better seen in Figure 2c where we plot the difference between the intensities $I(2\theta)$ collected at 75 s and 5 s. From Figure 2c a negative shift is deduced, indicating that the out-of-plane [110] direction of the FeRh film, under a constant V-bias, expands with time. The time-dependent XRD experiment was repeated for several t_s and V. The position of the (110) reflection [2θ(110)] was determined by a Gaussian fit of the corresponding $I(2\theta)$ data. In Figures 2d,e,f we plot 2θ(110) as a function of time for data recorded after application of 60 V, 65 V and 100 V, respectively. For 60 V (Figure 2d) the 2θ(110) increases up to a certain value with respect to its value at 0 V (dashed line) and remains constant, in accordance with the steady response found for $V \leq 60$ V. For $V = 65$ V (Figure 2e), the initial 2θ(110) position suddenly increases (with respect to its value at 0 V) and it progressively decreases with time afterwards. Notice that after applying 100 V (Figure 2f) 2θ(110) does not vary at all. Complementary XRD (see Supporting Information Figure S6) allow disregarding any substrate contribution to the observed relaxation.[25-26] Therefore, the obvious time-dependent position of the 2θ(110) must be related to the dynamics of the FM to AFM phase transition. Hence, it can be concluded that the AFM to FM phase transition takes place when certain bias-V is applied, more efficiently at $V \approx V_C$, but it partially reverses after a certain time

for sufficiently high voltages ($V > V_C$), leading to the observed decrease of magnetization and thus giving rise to a transient magnetoelectric response (Figure 1c).

To rationalize the experimental observation, we will refer to the sketches shown in **Figure 3.** Figure 3a summarizes the variation of *V*-induced strain (ε), mediated by PMNPT, acting on the FeRh film. We recall that due to the different unit cell volumes of the AFM and FM phases of FeRh, the FM phase is favored when the substrate induces an expansion of the FeRh film, being the effect maximum at the coercive voltage (V_C, Figure 2a). For $V << V_C$ (① the FeRh sample is largely in a AFM state with residual FM regions whose amount depends on the initial sample preparation conditions. In this case, an electric bias does not promote the formation/enlargement of the FM regions (Figure 3b). When *V* approaches V_C, path ①to ②in Figure 3a, the film crosses a certain critical strain value (ε_c) for which the AFM to FM phase transformation is favored. Therefore, new FM domains grow at expense of the neighboring AFM matrix. Pre-existing FM nuclei act as magnetic seeds and dictate the magnetization direction of the newly formed FM regions; the magnetic moment increases and remains constant (Figure 3c). Starting again from ① and applying larger bias voltages ($V >> V_C$), ε_c is crossed twice. While the first ε_c crossing signals the formation of the FM phase (①to ②path in Figure 3a, and Figure 3d), at the second ε_c crossing, the reverse FM-to-AFM transition shall occur (②to ③path in Figure 3a and sketch in Figure 3e). Therefore, the magnetic moment shall decrease and eventually recover its initial value (Figure 3f), which results in the observation of the $m(t)$ peak. The AFM to FM to AFM phase-transformation is, to some extent, slowed down by the inherent viscosity of the martensitic phase transformations (see Supporting Information Figure S7).[27] Dynamic responses have also been reported in multiferroic composites, due to electromechanical resonances[28] or due to

Maxwell-Wagner relaxation;[29] however, none of these situations apply in the system explored here.

A direct evidence of the presented scenario can be obtained by imaging the electric field dependence of the magnetic domains. With this purpose, X-Ray Magnetic Circular Dichroism combined with Photoelectron Emission Microscopy (XMCD–PEEM) experiments were performed (see Supporting Information Figure S8).[30] Experimental protocol for setting the initial state of the sample is described in Supporting Information Figure S1. Figures 4a,b show the 2x2 μm^2 XMCD images recorded under sample electrical bias at V=*-100* V and $V=V_C$. Comparison of Figures 4b and 4b show that red and blue regions (left/right poles of ferromagnetic regions) grow in Figure 4b compared with those of Figure 4a at expenses of the colorless (white regions), corresponding to regions with AFM order or regions where the net magnetization is perpendicular to incoming photon beam (red and blue regions). For instance, notice that the domains labeled with ① and ② expand under $V = V_C$ (Figure 4b) compared to V=-100 V (Figure 4a). These experimental results confirm the hypothesis that FM nuclei dictate the magnetization direction of the newly formed FM regions. In the case of the domain labelled with ③, its expansion is even more evident; in fact, the adjacent domain labelled with ③′ reverses its magnetic moment by 180^o after the expansion of the domain ③. Time-dependent XMCD-PEEM experiments allow reproducing the DME response, without spatial resolution enough to infer the domain dynamics (see Supporting Information Figure S9).

Conclusions

In conclusion, we have demonstrated that depending on the magnitude of an applied voltage, either steady or time-depending magnetoelectric responses of tailored magnitude can be obtained, and that this phenomenon results from the distinct slow dynamics of the AFM/FM martensitic phase transformation in FeRh. The experiments reported here have been performed at 110 °C, which is close to T_N of the stoichiometric FeRh films explored here. It is known that T_N of FeRh can be easily lowered by doping.[31-33] Therefore, similar effects could be easily obtained at room temperature. The reported robust and transient magnetoelectric effects are particularly appealing in emerging research fields such as spintronic logics or synapsis. In bioinspired computers, materials with tunable nonlinear response are searched to mimic time-dependent neuronal responses;[33] therefore, use of FeRh-based magnetoelectric devices in a network of similar devices may allow complex dynamic responses, such as synchronization

ASSOCIATED CONTENT

Supporting Information.

Experimental details, methods for sample preparation and complementary magnetic, magnetoelectric, structural characterization, and XMCD-PEEM are included.

AUTHOR INFORMATION

Corresponding Author

*ignasifinamartinez@gmail.com

Author Contributions

I.F., X.M. and J.S. designed the experiments. I.F. and F.S. were responsible of samples preparation the samples. I.F. prepared the experimental set-up for magnetoelectric characterization. I.F and A.Q. performed the magnetoelectric experiments. I.F. and J.-P.P. performed X-ray diffraction experiments. I.F., A.Q., F.M., M.F., and L.A. carried out XMCD-PEEM experiments. I.F., J.S. and J.F. wrote the manuscript. All authors contributed to and revised the manuscript.

Notes

The authors declare no competing financial interest.

ACKNOWLEDGMENTS

Financial support by the Spanish Government [Projects MAT2014-56063-C2-1-R, MAT2015-73839-JIN, MAT2014-51778-C2-1-R and MAT2014-57960-C3-1-R, MAT2015-64110-C2-2-P, and associated FEDER], the Generalitat de Catalunya (2014-SGR-734, 2014-SGR-1015) and the

European Research Council (SPIN-PORICS 2014-Consolidator Grant, Agreement nº 648454) is acknowledged. We also acknowledge support from the EU ERC Advanced Grant No. 268066, from the Ministry of Education of the Czech Republic Grant No. LM2011026, from the Grant Agency of the Czech Republic Grant no. 14-37427. ICMAB-CSIC authors acknowledge financial support from the Spanish Ministry of Economy and Competitiveness, through the "Severo Ochoa" Programme for Centres of Excellence in R&D (SEV- 2015-0496). IF acknowledges Juan de la Cierva – Incorporación postdoctoral fellowship (IJCI-2014-19102) from the Spanish Ministry of Economy and Competitiveness. Jose Santiso and Jose Manuel Caicedo Roque from Institut Català de Nanociència i Nanotecnologia are acknowledged for valuable collaboration on time-dependent X-ray characterization. We also acknowledge Max Stengel and Umesh Bhaskar for fruitful discussions.

REFERENCES

(1) Matsukura, F.; Tokura, Y.; Ohno, H., Control of Magnetism by Electric Fields. *Nat. Nanotechnol.* **2015,** *10* (3), 209-220.

(2) Martin, L.; Crane, S.; Chu, Y.; Holcomb, M.; Gajek, M.; Huijben, M.; Yang, C.; Balke, N.; Ramesh, R., Multiferroics and Magnetoelectrics: Thin Films and Nanostructures. *J. Phys.: Condens. Matter* **2008,** *20* (43), 434220.

(3) Ma, J.; Hu, J.; Li, Z.; Nan, C. W., Recent Progress in Multiferroic Magnetoelectric Composites: from Bulk to Thin Films. *Adv. Mater.* **2011,** *23* (9), 1062-1087.

(4) Vaz, C. A. F., Electric Field Control of Magnetism in Multiferroic Heterostructures. *J. Phys.: Condens. Matter* **2012,** *24* (33), 333201.

(5) Ortega, N.; Kumar, A.; Scott, J.; Katiyar, R. S., Multifunctional Magnetoelectric Materials for Device Applications. *J. Phys.: Condens. Matter* **2015,** *27* (50), 504002.

(6) Senff, D.; Link, P.; Aliouane, N.; Argyriou, D.; Braden, M., Field Dependence of Magnetic Correlations through the Polarization Flop Transition in Multiferroic $TbMnO_3$: Evidence for a Magnetic Memory Effect. *Phys. Rev. B* **2008,** *77* (17), 174419.

(7) Taniguchi, K.; Abe, N.; Ohtani, S.; Arima, T., Magnetoelectric Memory Effect of the Nonpolar Phase with Collinear Spin Structure in Multiferroic $MnWO_4$. *Phys. Rev. Lett.* **2009,** *102* (14), 147201.

(8) Finger, T.; Senff, D.; Schmalzl, K.; Schmidt, W.; Regnault, L.; Becker, P.; Bohatỳ, L.; Braden, M., Electric-Field Control of The Chiral Magnetism of Multiferroic $MnWO_4$ As Seen Via Polarized Neutron Diffraction. *Phys. Rev. B* **2010,** *81* (5), 054430.

(9) Fina, I.; Fabrega, L.; Marti, X.; Sanchez, F.; Fontcuberta, J., Chiral Domains in Cycloidal Multiferroic Thin Films: Switching and Memory Effects. *Phys. Rev. Lett.* **2011,** *107* (25), 257601.

(10) Tokura, Y.; Kida, N., Dynamical Magnetoelectric Effects in Multiferroic Oxides. *Philos. Trans. R. Soc.,* A **2011,** *369* (1951), 3679-3694.

(11) Pimenov, A.; Mukhin, A.; Ivanov, V. Y.; Travkin, V.; Balbashov, A.; Loidl, A., Possible Evidence for Electromagnons in Multiferroic Manganites. *Nat. Phys.* **2006,** *2* (2), 97-100.

(12) Hu, J. M.; Li, Z.; Chen, L. Q.; Nan, C. W., Design of a Voltage-Controlled Magnetic Random Access Memory Based on Anisotropic Magnetoresistance in a Single Magnetic Layer. *Adv. Mater.* **2012,** *24* (21), 2869-2873.

(13) Maat, S.; Thiele, J. U.; Fullerton, E. E., Temperature and Field Hysteresis of the Antiferromagnetic-to-Ferromagnetic Phase Transition in Epitaxial FeRh films. *Phys. Rev. B* **2005,** *72* (21), 214432.

(14) Mariager, S.; Guyader, L. L.; Buzzi, M.; Ingold, G.; Quitmann, C., Imaging the Antiferromagnetic to Ferromagnetic First Order Phase Transition of FeRh. *arXiv preprint arXiv:1301.4164* **2013**.

(15) Zakharov, A. I., Kadomtseva, A. M., Levitin, R. Z. & Ponyatovskii, E. G. Magnetic and Magnetoelastic Properties of a Metamagnetic Iron–Rhodium Alloy. *J. Exp. Theor. Phys.* 19, 1348 (1964).

(16) Lee, Y.; Liu, Z.; Heron, J.; Clarkson, J.; Hong, J.; Ko, C.; Biegalski, M.; Aschauer, U.; Hsu, S.-L.; Nowakowski, M., Large Resistivity Modulation in Mixed-Phase Metallic Systems. *Nat. Commun.* **2015,** *6*, 5959

(17) Liu, Z.; Li, L.; Gai, Z.; Clarkson, J.; Hsu, S.; Wong, A.; Fan, L.; Lin, M.-W.; Rouleau, C.; Ward, T., Full Electroresistance Modulation in a Mixed-Phase Metallic Alloy. *Phys. Rev. Lett.* **2016,** *116* (9), 097203.

(18) Moya, X.; Kar-Narayan, S.; Mathur, N., Caloric Materials near Ferroic Phase Transitions. *Nat. Mater.* **2014,** *13* (5), 439-450.

(19) Cherifi, R. O.; Ivanovskaya, V.; Phillips, L. C.; Zobelli, A.; Infante, I. C.; Jacquet, E.; Garcia, V.; Fusil, S.; Briddon, P. R.; Guiblin, N.; Mougin, A.; Ünal, A. A.; Kronast, F.; Valencia, S.; Dkhil, B.; Barthélémy, A.; Bibes, M., Electric-Field Control of Magnetic Order Above Room Temperature. *Nat. Mater.* **2014,** *13* (4), 345-351.

(20) Phillips, L.; Cherifi, R. O.; Ivanovskaya, V.; Zobelli, A.; Infante, I. C.; Jacquet, E.; Guiblin, N.; Unal, A. A.; Kronast, F.; Dkhil, B., Local Electrical Control of Magnetic Order and Orientation by Ferroelastic Domain Arrangements just above Room Temperature. *Sci Rep.* **2014,** *5*, 10026.

(21) Clarkson, J.; Frontera, C.; Liu, Z.; Lee, Y.; Kim, J.; Cordero, K.; Wizotsky, S.; Sanchez, F.; Sort, J.; Hsu, S., An Invisible Non-Volatile Solid-State Memory. *preprint arXiv:1604.03383* **2016**.

(22) Bauer, U., Yao, L., Tan, A. J., Agrawal, P., Emori, S., Tuller, H. L., van Dijken, S., Beach, G. S. Magneto-Ionic Control of Interfacial Magnetism. *Nat. Mater.* **2015**, 14(2), 174-181.

(23) Gilbert, D. A., Olamit, J., Dumas, R. K., Kirby, B. J., Grutter, A. J., Maranville, B. B., Arenholz, E., Borchers, J.A., Liu, K.Controllable Positive Exchange Bias via Redox-Driven Oxygen Migration. *Nat. Commun.* **2016**, 7, 11050.

(24) Gilbert, D. A., Grutter, A. J., Arenholz, E., Liu, K., Kirby, B. J., Borchers, J. A., & Maranville, B. B. (2016). Structural and Magnetic Depth Profiles of Magneto-Ionic Heterostructures Beyond the Interface Limit. *Nat. Commun.* **2016** 7, 12264.

(25) Ishchuk, V.; Samoylenko, Z.; Sobolev, V., The Kinetics of the Local Compositional Changes at the Ferroelectric–Antiferroelectric Interphase Boundaries in Lead–Lanthanum Titanate–Zirconate Solid Solutions. *J. Phys.: Condens. Matter* **2006,** *18* (49), 11371.

(26) Vasudevan, R. K.; Zhang, S.; Okatan, M. B.; Jesse, S.; Kalinin, S. V.; Bassiri-Gharb, N., Multidimensional Dynamic Piezoresponse Measurements: Unraveling Local Eelaxation Behavior in Relaxor-Ferroelectrics via Big Data. *J. Appl. Phys.* **2015,** *118* (7), 072003.

(27) Chattopadhyay, M.; Roy, S.; Nigam, A.; Sokhey, K.; Chaddah, P., Metastability and Giant Relaxation Across the Ferromagnetic to Antiferromagnetic Transition in Ce (Fe 0.96 Ru 0.04) 2. *Phys. Rev. B* **2003,** *68* (17), 174404.

(28) Zhai, J., Xing, Z., Dong, S., Li, J. and Viehland, D. Magnetoelectric Laminate Composites: An Overview. *J. Am. Ceram. Soc.* **2008**, 91, 351 (2008)]

(29) Petrov, V. M., Bichurin, M. I., Srinivasan, G., Zhai, J., Viehland, D. Dispersion Characteristics for Low-Frequency Magnetoelectric Coefficients in Bulk Ferrite-Piezoelectric Composites. Solid State Commun. **2007**, 142(9), 515-518.

(30) Aballe, L., Foerster, M., Pellegrin, E., Nicolas, J., Ferrer, S., The ALBA spectroscopic LEEM-PEEM experimental station: layout and performance. *J. Synchrotron Radiat.* **2015**, 22, 745–752.

(31) Suzuki, I.; Itoh, M.; Taniyama, T., Elastically Controlled Magnetic Phase Transition in Ga-FeRh/BaTiO 3(001) Heterostructure. *Appl. Phys. Lett.* **2014,** *104* (2), 022401.

(32) Wayne, R., Pressure Dependence of the Magnetic Transitions in Fe-Rh alloys. *Phys. Rev.* **1968,** *170* (2), 523.

(33) Lewis, L.; Marrows, C.; Langridge, S., Coupled Magnetic, Structural, and Electronic Phase Transitions in FeRh. *J. Phys. D: Appl. Phys.* **2016,** *49* (32), 323002.

(34) Grollier, J., Querlioz, D., & Stiles, M. D. Spintronic Nanodevices for Bioinspired Computing. *Proc. IEEE* **2016**, 104(10), 2024-2039.

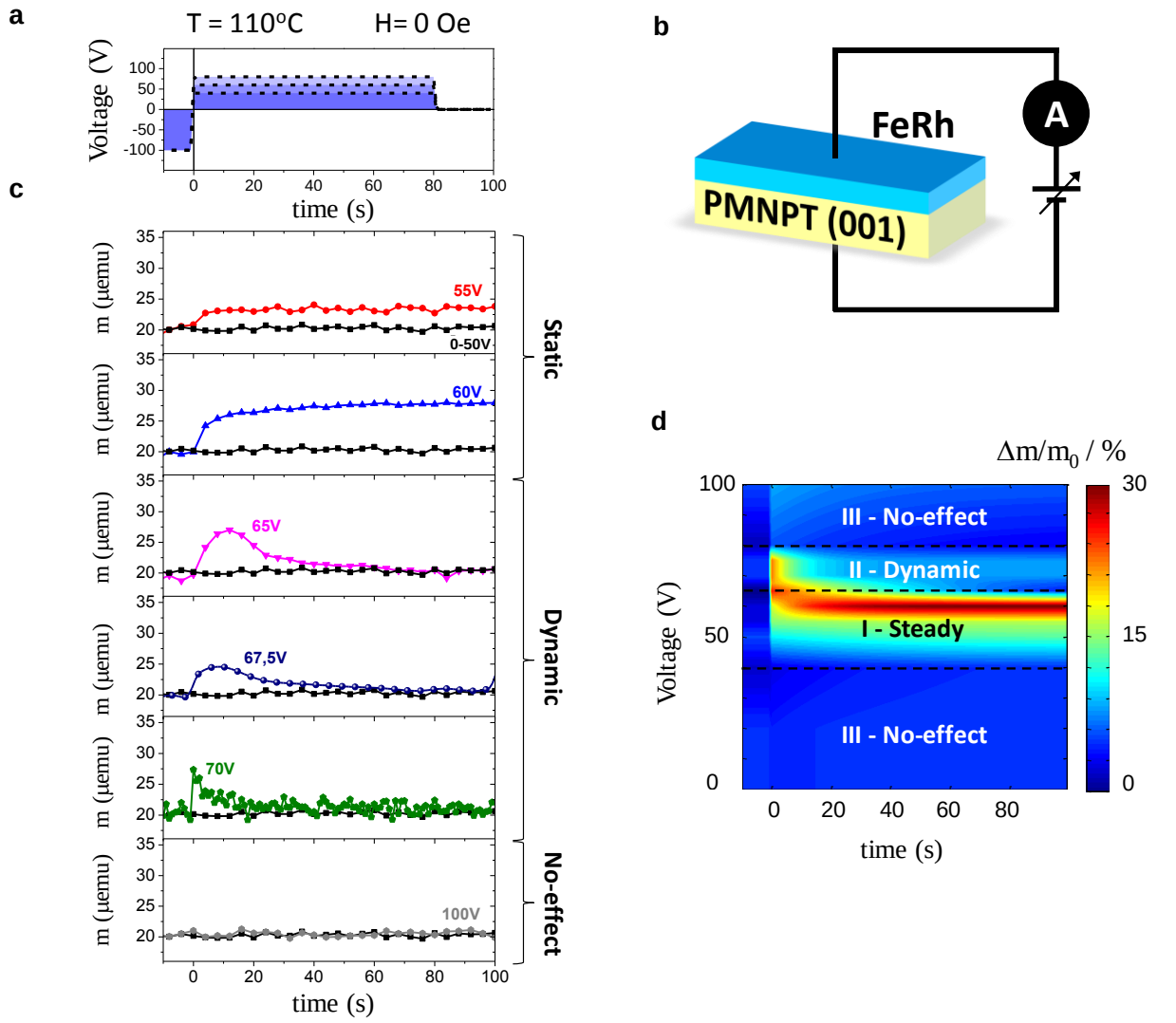

Figure 1. (a) Illustrative applied voltage vs. time profile. (b) Sketch of the /PMNPT structure and the electric contact configuration. (c) Time-dependent magnetic moment $m(t,V)$ for different applied voltages as illustrated in (a). (d) Color map of the relative change of magnetic moment [$\Delta m/m_0 = (m - m_0)/m_0$ (m_0 is the magnetic moment at t = 0 s)] depending on the applied electric voltage and time. The different regions (I, II and III) where the magnetoelectric effect is "steady", "dynamic" or "no-effect" are indicated.

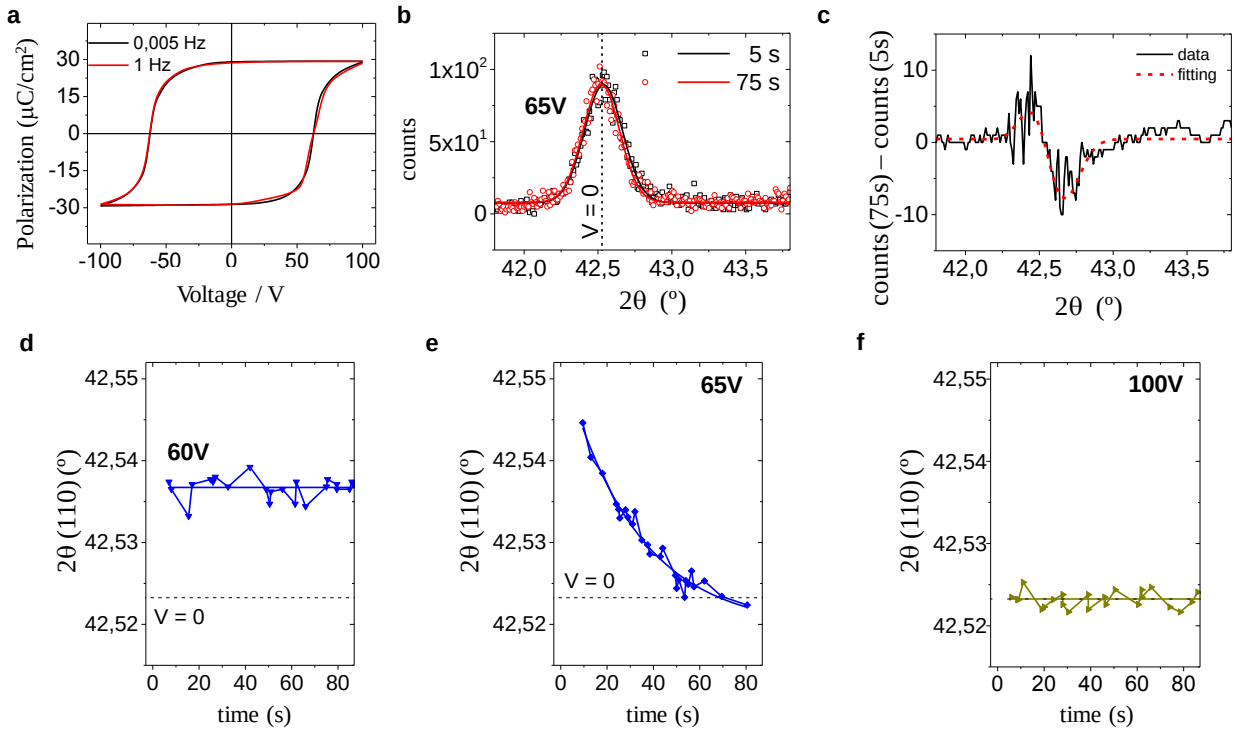

Figure 2. (a) Polarization versus voltage loops measured at 0.005 and 1 Hz, at 110ºC, using the electric contact configuration shown in Figure 1b. (b) Scan around the FeRh (110) reflection for different delay times after applying +65 V. (c) Difference between the scan recorded after 75 s (averaging with a 0.1^{o} window) and the one recorded after 5 s (solid line). (d) Time-dependent FeRh (110) peak position $2\theta(110)$ as a function of the delay time after switching on the bias 60 V. A pre-poling field of -100 V was used. Lines through data are a guide for the eye. (e) Equivalent to (d) after applying $V = 65$ V. (f) Equivalent to (d) after applying $V = 100$ V.

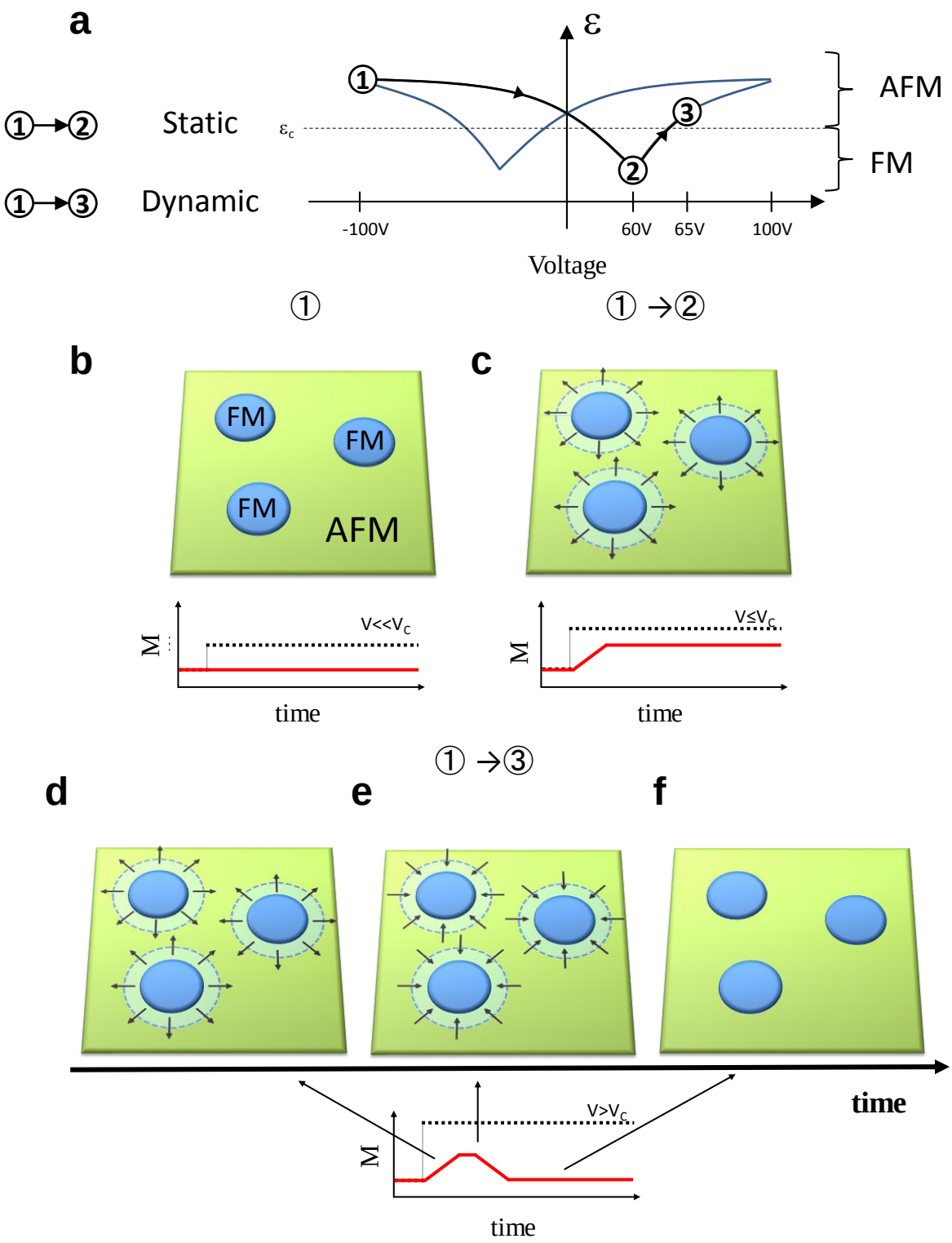

Figure 3. (a) Sketch of the substrate induced film strain response on applied voltage. After poling in the static regime, for voltages ≤ 60 V (①to ②) the FM to AFM transition takes place

from a certain critical strain (ε_c). If, after poling, the voltage is > 60 V (①to ③) ε_c is crossed twice producing an AFM→FM→AFM double phase transition, as experimentally observed. (b) Sketch of the coexisting FM and AFM phases at the initial state or for any applied voltage $<<V_C$ (①). (c) Sketch of the increase of FM domains at expenses of AFM ones for applied voltages just below or equal to V_C (① to ②). (d,e) Expansion (at d) and further compression (at e) of the FM domains during the transient magnetoelectric response for voltages just above V_C. (f) final recovery of the initial state (① to ③).

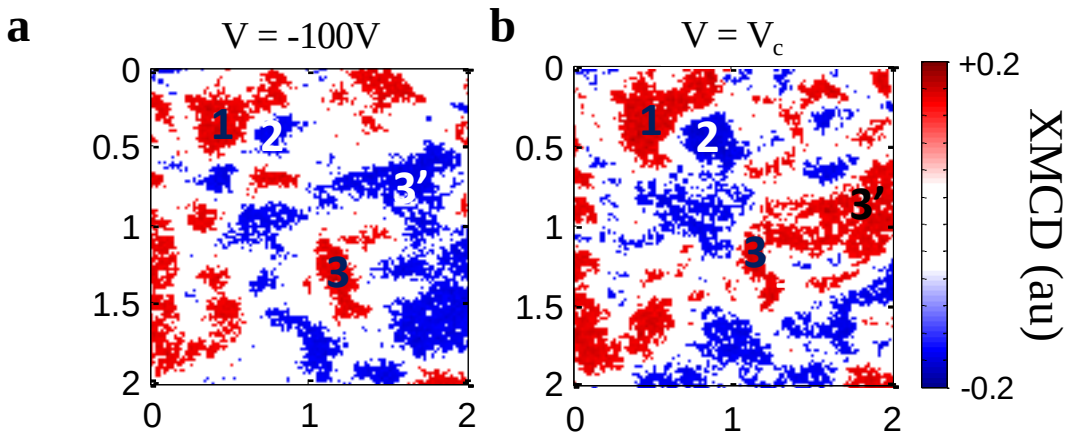

Figure 4. (a,b) PEEM-XMCD image collected in the very same region at V = -100 V and at $V = V_C$, respectively. The false color scale corresponds to the projection of the magnetization onto the incident x-ray beam direction (horizontal from the left). Domains with magnetization parallel and antiparallel to the x-ray incidence have opposite contrast (blue and red colors). Perpendicular domains or domains with zero magnetic moment have white color. Images correspond to 2 μm lateral size.

Table of contents graph: